Journal of Solid State Chemistry 184 (2011) 1843–1849

Contents lists available at ScienceDirect

Journal of Solid State Chemistry

journal homepage: www.elsevier.com/locate/jssc

# $Y(P,V)O_4:Dy^{3+}$ phosphors for white light generation: Emission dynamics and host effect

Fabio Angiuli, Francesco Mezzadri, Enrico Cavalli *

*Dipartimento di Chimica Generale ed Inorganica, Chimica Analitica, Chimica Fisica, Università di Parma, viale Usberti 17/a 43100 Parma, Italy*

ARTICLE INFO

*Article history:*
Received 25 February 2011
Received in revised form
19 May 2011
Accepted 20 May 2011
Available online 30 May 2011

*Keywords:*
White light emitting phosphors
$Dy^{3+}$ emission
Luminescent materials

ABSTRACT

The structural characteristics and optical spectra of $Y(P,V)O_4:Dy^{3+}$ phosphors obtained by solid state reaction, sol–gel and hydrothermal routes have been investigated and compared. The luminescence features of these materials show a complicate dependence on the composition, synthetic method and excitation conditions. The emission performance depends on different effects: host luminescence, energy transfer to the doping ions and host dependence of the $Dy^{3+}$ emission properties. These effects have been rationalized in order to provide useful information for the development of a suitable material for the white light emitting phosphors technology.



## 1. Introduction

The possibility of modulating the emission properties of a rare earth based phosphor by playing with the host composition and the interaction processes between the active ions allows to individuate strategies for tailoring the performances of the material [1]. Their application to the development of white light emitting phosphors has produced interesting results. The luminescence spectra of these compounds present emission bands in the blue and yellow (or red) regions with appropriate relative intensities. This combination has been realized for instance in $Eu^{2+}/Mn^{2+}$ or $Ce^{3+}/Mn^{2+}$ co-doped phosphors [2,3], whose syntheses require the accurate control of the experimental conditions in order to avoid the formation of unwanted optical centers like $Eu^{3+}$ and $Ce^{4+}$. Recent studies have demonstrated that $Dy^{3+}$-doped phospho-vanadate lattices could constitute interesting alternative materials [4,5]. Their emission spectra present the blue (480 nm), yellow (570 nm) and red (660 nm, weak) bands of $Dy^{3+}$ superimposed to the blue host emission. Bao et al. [4] have synthesized by the Pechini sol–gel method a series of phosphors with general formula $Y_{1-y}Dy_y(P_xV_{1-x})O_4$ and investigated their luminescence properties as a function of the host composition and of the doping concentration, concluding that the $Y_{0.99}Dy_{0.01}(P_{0.8}V_{0.2})O_4$ system is very promising for applications as a white phosphor and that further work is necessary in order to optimize its performance. Starting from these results we have decided to deepen the study of this kind of materials in order to better understand the effect of the host characteristics on the emission properties. We have taken into consideration three different synthetic methodologies and verified their impact on the luminescence performances. We have also investigated the processes governing the emission dynamics in these systems and pointed out the role of the host lattice characteristics formalized in the framework of the Judd–Ofelt theory.

## 2. Experimental

### 2.1. Synthesis

$Y_2O_3$ (Aldrich, 99.99%), $(NH_4)H_2PO_4$ (Merck, 99%), $NH_4VO_3$ (Riedel-deHaën, 98.5%) and $Dy_2O_3$ (Aldrich, 99.9%) were used as starting materials. A series of compounds with general formula $Y_{0.99}Dy_{0.01}(P_xV_{1-x})O_4$ ($x=0$, 0.2, 0.5, 0.8, 1) were synthesized 'via' solid state reaction: stoichiometric amounts of the precursors were thoroughly mixed in alumina crucible, pre-sintered at 500 °C for 2 h and then calcined at 1200 °C for 12 h. The hydrothermal and the sol–gel Pechini methods were then applied to the synthesis of the $Y_{0.99}Dy_{0.01}$ $(P_{0.8}V_{0.2})O_4$ phosphor. The starting solution for both procedures was obtained after dissolution of the components in $HNO_3$ 3 M at 75 °C under vigorous stirring and addition of citric acid as chelating agent. In the hydrothermal route, the obtained mixture was poured into a Teflon-lined stainless steel autoclave (60% filling) and heated at 180 °C for 12 h. The resulting suspension was then washed several times with distilled water and then centrifuged. The separated powder was dried at 120 °C for 1 h and then heated at 500 °C for 2 h and successively annealed at 900 °C for t2 h. In the Pechini procedure the gel, obtained after addition of PEG (20% w/w) to the starting solution, was dried at 120 °C for 12 h and then thermally treated as in the previous case.

Table 1 reports the list of the synthesized samples and the acronyms used along the paper.

* Corresponding author.
*E-mail addresses:* fabio.angiuli@nemo.unipr.it (F. Angiuli), francesco.mezzadri@unipr.it (F. Mezzadri), enrico.cavalli@unipr.it (E. Cavalli).

0022-4596/$ - see front matter © 2011 Elsevier Inc. All rights reserved.
doi:10.1016/j.jssc.2011.05.027

### 2.2. Characterization

The samples were characterized by XRD powder diffraction using a Thermo ARL X'tra diffractometer equipped with a Si(Li) Thermo Electron solid state detector with Cu$K\alpha$ radiation. The morphology of the phosphors particles was examined by means of a 515 Philips scanning electron microscope (SEM).

The room temperature emission and excitation spectra were measured using a Fluoromax-3 (Jobin-Yvon) spectrofluorimeter. The decay profiles were measured at 300 K upon 355 nm laser excitation using a pulsed Nd:YAG laser (Quanta System model SYL 202); the emission was isolated by means of a Hilger–Watts Model D330 double monochromator and detected with a Hamamatsu R943-022 photomultiplier connected to a LeCroy 9410 transient digitizer.

## 3. Results and discussion

### 3.1. Solid state synthesis and host effects on the luminescence properties

The samples obtained by solid state reaction were used to investigate the crystallographic and emission properties as a function of the host composition. Their powder X-Ray diffraction (PXRD) patterns, reported in Fig. 1(a), are characterized by a progressive shift of the peaks towards lower $2\theta$ values with increasing vanadium concentration. A close inspection of the patterns has revealed that the occasional presence of extra phases, mostly unreacted $V_2O_5$, does not exceed 1% of the total amount. A refinement by the Rietveld method was been carried out using the GSAS package [6,7] in the $I4_1/amd$ space group (zircon-type structure). The agreement between measured and calculated intensities was good, (see the Rietveld plot of Fig. 1(b) as an example). The most relevant parameters resulting from the refinements are collected in Table 2. They are consistent with those previously published [8,9]. The evaluated mean bond lengths are reported in Table 3. As expected, the yttrium–oxygen distances slightly increase (no more than 1% in total), while the average phosphor/vanadium–oxygen distances progressively increase (up to about 10%) with the vanadium concentration, consistently with the individual bond lengths reported for the tetrahedrally coordinated $P^{5+}$ and $V^{5+}$ cations (1.52 and 1.70 Å, respectively, [10]). The SEM image of the $SS_2D_1$ phosphor, Fig. 1(c), reveals that it is composed of micrometric grains having roundish contours, as a consequence of the partial sintering process taking place during the solid state reaction occurring at relatively high temperature (1200 °C). The visible emission spectra of the $Dy^{3+}$ ion in oxide lattices are composed of two main bands in the blue (480 nm) and yellow (575 nm) region and of a weaker feature in the red, assigned to the transition from the $^4F_{9/2}$ level to $^6H_{15/2}$, $^6H_{13/2}$, and $^6H_{11/2}$, respectively. Bao et al. [4] have observed that the relative intensity of the yellow and blue bands (expressed as Y/B ratio) depends on the host composition and is in great part responsible for the color of the emitted radiation. We have discussed this aspect by considering the results of the Judd–Ofelt (J–O) theory [11,12] applied to the analysis of the absorption spectra of $Dy^{3+}$ in $YVO_4$ and $YPO_4$ single crystals [13,14]. The oscillator strengths of the absorption transitions can be reproduced by means of three parameters ($\Omega_n$, $n=2, 4, 6$), referred to as intensity or J–O parameters,

**Table 1**
List of the synthesized samples and identifying acronyms.

| Phosphor | Synthetic technique | Acronym |
|---|---|---|
| $Y_{0.99}Dy_{0.01}PO_4$ | Solid state reaction | $SS_1D_1$ |
| $Y_{0.99}Dy_{0.01}(P_{0.8}V_{0.2})O_4$ | Solid state reaction | $SS_2D_1$ |
| $Y_{0.99}Dy_{0.01}(P_{0.5}V_{0.5})O_4$ | Solid state reaction | $SS_3D_1$ |
| $Y_{0.99}Dy_{0.01}(P_{0.2}V_{0.8})O_4$ | Solid state reaction | $SS_4D_1$ |
| $Y_{0.99}Dy_{0.01}VO_4$ | Solid state reaction | $SS_5D_1$ |
| $Y_{0.99}Dy_{0.01}(P_{0.8}V_{0.2})O_4$ | Hydrothermal method | $HTD_1$ |
| $Y_{0.99}Dy_{0.01}(P_{0.8}V_{0.2})O_4$ | Sol–gel | $SGD_1$ |

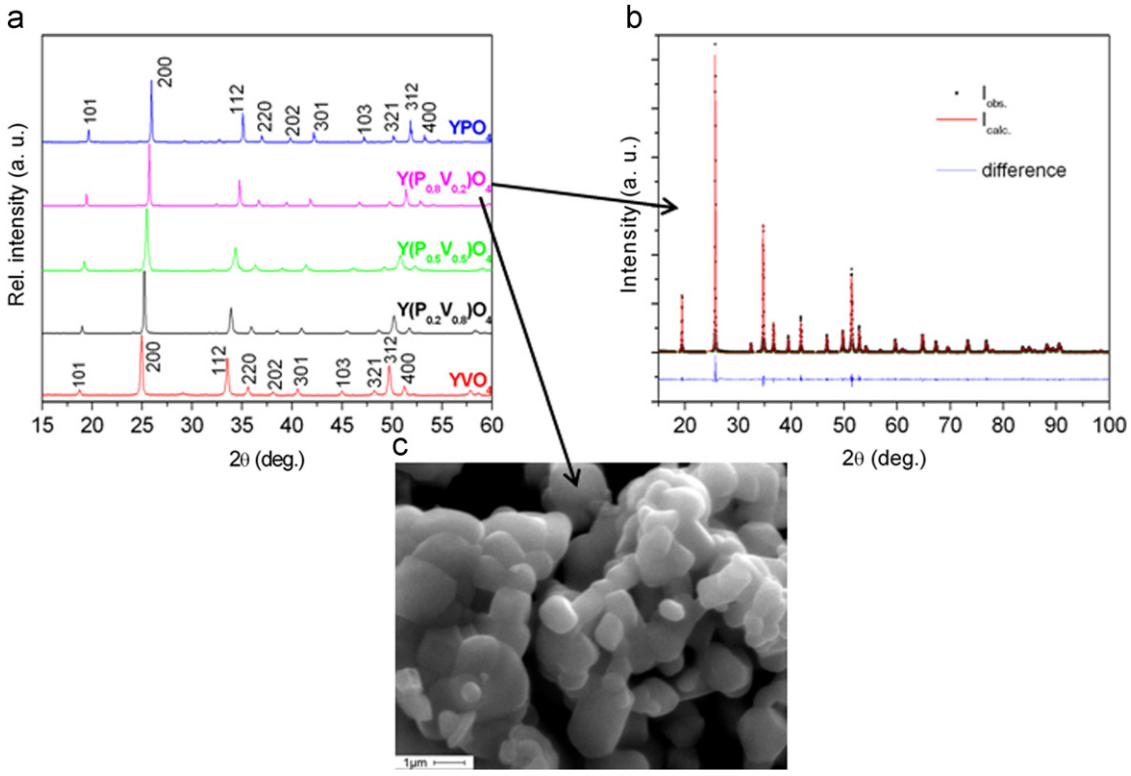


**Fig. 1.** (a) PXRD patterns along the $Y_{0.99}Dy_{0.01}(P_{1-x}V_x)O_4$ system synthesized by solid state reaction. (b) Rietveld plot and (c) SEM image of the $SS_2D_1$ sample.

**Table 2**
Results of the Rietveld refinement of the XRD patterns of Fig. 1. All the refinements have been carried out in the $I4_1/amd$ space group with the yttrium atom located at (0, 1/4, −1/8), the phosphor (vanadium) at (0, 1/4, 3/8) and the oxygen at (0, $y$, $z$).

| Sample | Lattice parameters | | | Refined P occupancy | Atomic coordinates | | Isotropic thermal parameters (Å$^2$) | | | $R(F^2)$ | $\chi^2$ |
|---|---|---|---|---|---|---|---|---|---|---|---|
| | $a=b$ (Å) | $c$ (Å) | $V$ (Å$^3$) | | O $y$ | O $z$ | Y | P/V | O | | |
| $SS_1D_1$ | 6.885(1) | 6.022(1) | 285.45(2) | 0.99(1) | 0.075(1) | 0.213(1) | 0.006(1) | 0.008(1) | 0.003(1) | 5.35 | 1.95 |
| $SS_2D_1$ | 6.929(1) | 6.073(1) | 291.66(2) | 0.84(2) | 0.075(1) | 0.213(1) | 0.009(1) | 0.006(2) | 0.006(2) | 3.31 | 5.83 |
| $SS_3D_1$ | 6.987(1) | 6.138(1) | 299.63(2) | 0.58(1) | 0.078(1) | 0.208(1) | 0.004(1) | 0.004(1) | 0.007(1) | 5.86 | 7.25 |
| $SS_4D_1$ | 7.072(1) | 6.239(1) | 311.98(1) | 0.26(1) | 0.071(3) | 0.206(1) | 0.011(1) | 0.004(1) | 0.006(1) | 5.06 | 5.94 |
| $SS_5D_1$ | 7.119(1) | 6.292(1) | 318.92(1) | 0.01(1) | 0.434(1) | 0.202(1) | 0.005(1) | 0.007(1) | 0.007(1) | 5.53 | 0.65 |

**Table 3**
Relevant bond distances.

| Sample | Y–O avg. distance | (P,V)–O avg. distance |
|---|---|---|
| $SS_1D_1$ | 2.346(1) | 1.551(1) |
| $SS_2D_1$ | 2.358(1) | 1.562(1) |
| $SS_3D_1$ | 2.365(1) | 1.583(1) |
| $SS_4D_1$ | 2.371(1) | 1.648(1) |
| $SS_5D_1$ | 2.369(1) | 1.704(1) |

whose values can be determined through a least square fitting procedure. These parameters can then be used to calculate the spontaneous emission probabilities, the radiative branching ratios and the radiative lifetimes of the emitting levels. Theoretical principles and calculation details are well documented in literature [15] and not reported here. Concerning the present context, Faoro et al. [14] pointed out that the vanadate host is characterized by much larger values of the $\Omega_2$ and $\Omega_4$ intensity parameters with respect to the phosphate lattice: this implies a higher value of the spontaneous emission coefficient of the $^4F_{9/2}$ emission, a shorter lifetime and a larger ratio between the spontaneous emission probabilities associated to the yellow and to the blue emission. In analogy with the $Eu^{3+}$:Y(P,V)$O_4$ case [16], we expect that these properties progressively vary with the composition along the $Y_{0.99}Dy_{0.01}(P_xV_{1-x})O_4$ isomorphic series. In Fig. 2(a) we compare the emission spectra of the $SS_nD_1$ ($n$=1–5) samples measured upon 390 nm excitation, in correspondence of the most intense $Dy^{3+}$ absorption transition. They have been normalized with respect to the maximum of the blue emission band. As expected, the Y/B intensity ratio and the total emission intensity increase with the vanadium content. The decay curves of the $Dy^{3+}$ emission are shown in Fig. 2(b): they are nearly single exponential for $x \le 0.2$ and non exponential for $x > 0.2$. Different factors can affect the emission decay profiles, like the presence of lattice defects, of non-equivalent emitting centers [16] as well as energy transfer processes, certainly active at the adopted doping level. The average decay times have been estimated by means of the formula [17]

$$\tau = \frac{\int tI(t)dt}{\int I(t)dt} \quad (1)$$

where $I(t)$ represents the luminescence intensity at time $t$. They are listed in Table 4, together with the radiative lifetimes of the $^4F_{9/2}$ level in the pure phosphate and vanadate hosts. In the same table the experimental values of the Y/B ratio, obtained from the integrated areas of the corresponding emission bands, are compared with the theoretical values calculated from the ratios of the appropriate spontaneous emission coefficients averaged over the host compositions. It is evident that the experimental data follows only qualitatively the trend individuated by the J–O approach, and that there is a significant discrepancy between the expected and the observed values. The intrinsic uncertainty of the model (of the order of ±30%), the possibility of calibration errors, the presence of defect centers and the non-radiative processes can only in part account for this discrepancy. On the other hand, it is well known that there are aspect of the spectroscopy of the $Dy^{3+}$-doped compounds that are not yet fully understood [18] and we do not exclude that further work in this direction could imply a revision of the J–O analysis applied to these materials. The average decay times evaluated using Eq. (1) take into account the effects of different optical centers and have the advantage of being comparable, then suitable for the previous considerations. However, a more accurate examination of the non exponential curves of Fig. 4 reveal that they have the profiles typically observed in the case of $Dy^{3+}$–$Dy^{3+}$ energy transfer processes [18,19] associated to resonant or nearly resonant cross relaxation mechanisms such as:

$$^4F_{9/2} + {}^6H_{15/2} \rightarrow {}^6H_{5/2} + {}^6F_{7/2}$$

$$^4F_{9/2} + {}^6H_{15/2} \rightarrow ({}^6F_{3/2}, {}^6F_{1/2}) + ({}^6H_{9/2}, {}^6F_{11/2})$$

schematized in Fig. 2(c). We have analyzed these decay curves by means of the Inokuti–Hirayama [20] model suitable for energy transfer processes in absence of migration among the donors

$$\phi(t) = A\exp\left[-\frac{t}{\tau} - \alpha\left(\frac{t}{\tau}\right)^{3/s}\right] \quad (2)$$

where $\phi(t)$ is the emission intensity after pulsed excitation, $A$ is the intensity of the emission at $t$=0, $\tau$ is the lifetime of the isolated donor, $\alpha$ is a parameter containing the energy transfer probability and $s$=6 for dipole–dipole (D–D), 8 for dipole–quadrupole (D–Q) and 10 for quadrupole–quadrupole (Q–Q) interaction. The best fit of the decay curves has been carried out on the basis of Eq. (2) by considering a D–D process and $A$,$\tau$ and $\alpha$ as adjustable parameters. The parameter $\alpha$ provides information on the probability of the energy transfer process

$$\alpha = \frac{4}{3}\pi\Gamma\left(1-\frac{3}{s}\right)N_aR_0^3 \quad (3)$$

where $\Gamma$ is the gamma function, $N_a$ the concentration of the acceptor expressed in ions · cm$^{-3}$ and $R_0$ is the critical distance for the transfer. The values of $\tau$ and of the critical distances deduced from the fit procedures are reported in Table 5, together with the average distances between the $Dy^{3+}$ ions calculated using the data reported in Table 2. These results raise interesting considerations. First of all, the lifetimes of the isolated donors are significantly longer than the average decay times calculated by means of Eq. (1): in the case of the pure phosphate the obtained value is very close, compatibly with the approximations involved, to that calculated by means of the J–O approach. This is not sufficient to account for the discrepancies between experimental and theoretical results, but it provides good indications in this direction. Second the critical distance for the energy transfer is of the same order of magnitude of the average distance between the doping ions when the radiative lifetime is long, i.e. for $x$=1 and 0.8, and significantly decreases for $x$=0.5. When the vanadium content exceeds that of phosphor in the host composition, the decay profile become exponential. We conclude that the probability of the $Dy^{3+}$–$Dy^{3+}$ energy transfer process increases with the

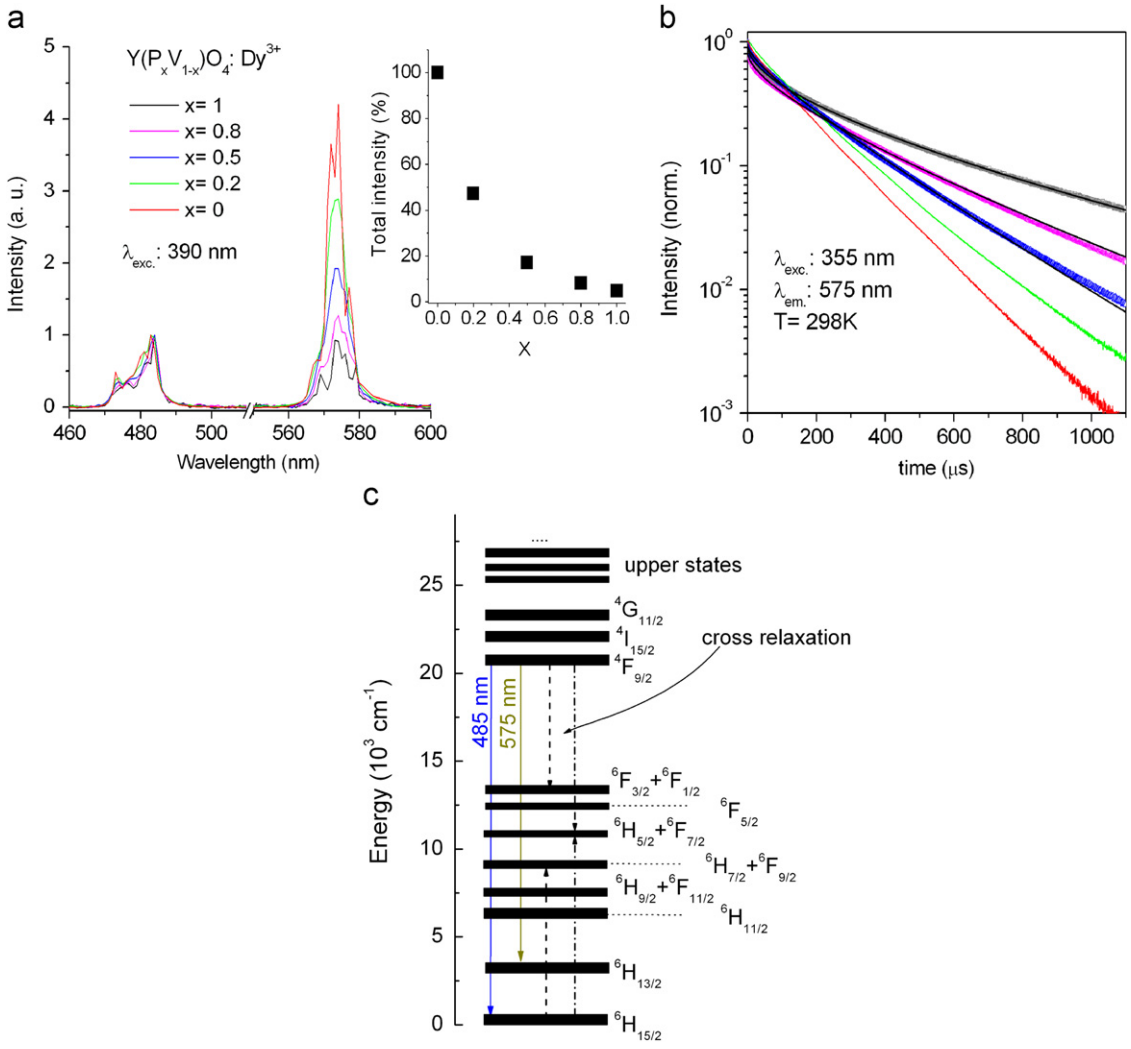


**Fig. 2.** (a) Emission spectra and (b) decay profiles of the $SS_nD_1$ samples (the black lines reproduce the Inokuti–Hirayama fit). In the inset the total intensity of the emission is reported as a function of the host composition. (c) Energy levels scheme of the $Dy^{3+}$ ion with the most important emission transitions and cross relaxation pathways.

**Table 4**
Radiative lifetimes and experimental decay times of the $^4F_{9/2}$ state, calculated and experimental Y/B ratios along the $Y_{0.99}Dy_{0.01}(P_xV_{1-x})O_4$ series.

| $x$ | $\tau$ (μs)$_{calc.}$ | $\tau$ (μs)$_{exp.}$ | Y/B$_{calc.}$ | Y/B$_{exp.}$ |
|---|---|---|---|---|
| 1 | 1279 | 485 | 1.36 | 0.76 |
| 0.8 | – | 315 | 1.91 | 1.06 |
| 0.5 | – | 232 | 2.74 | 1.45 |
| 0.2 | – | 182 | 3.57 | 1.89 |
| 0 | 440 | 150 | 4.12 | 2.28 |

Judd–Ofelt parameters.
$YPO_4 \rightarrow \Omega_2=0.51$, $\Omega_4=1.91$, $\Omega_6=2.87$ ($\times 10^{20}$ cm$^2$) from Ref. [14].
$YPO_4 \rightarrow \Omega_2=6.59$, $\Omega_4=3.71$, $\Omega_6=7.74$ ($\times 10^{20}$ cm$^2$) from Ref. [13].

**Table 5**
Lifetimes and critical distances for the $Dy^{3+}-Dy^{3+}$ energy transfer process in $Y_{0.99}Dy_{0.01}(P_xV_{1-x})O_4$ obtained from the Inokuti–Hirayama fit of the decay curves of Fig. 2(b).

| $x$ | $\tau_{rad.}$ (μs) | $d_{crit.}$ (Å) | $d_{av.}$ (Å) |
|---|---|---|---|
| 1 | 1346 | 13.4 | 11.9 |
| 0.8 | 589 | 11.2 | 12.0 |
| 0.5 | 306 | 9.1 | 12.1 |

intrinsic lifetime of the donor, namely with the P/V ratio. Excitation in the UV region is attractive in the perspective of applications in the phosphor technology. The excitation spectrum shown in Fig. 3(a) is constituted of a strong absorption edge starting at about 330 nm and extending in the UV, ascribed to the charge transfer transition of the vanadate units. The absorption features of $Dy^{3+}$ are much weaker and located at 352 ($^4M_{5/2}+{}^6P_{7/2}\leftarrow{}^6H_{15/2}$), 366 ($^4P_{3/2}+{}^6P_{3/2}\leftarrow{}^6H_{15/2}$) and 390 nm ($^4I_{13/2}+{}^4K_{17/2}\leftarrow{}^6H_{15/2}$). The relative intensity of the host band allows to infer that the energy transfer from the $VO_4^{3-}$ group to the $Dy^{3+}$ ion is rather efficient. Obviously this process does not take place in the pure phosphate lattice. In the emission spectra measured upon 280 nm excitation, shown in Fig. 3(a), the expected trends of both Y/B ratio and overall $Dy^{3+}$ luminescence intensity are confirmed. In addition, the spectra present the characteristic broadband vanadate emission in the blue region, with maximum at 440 nm. This band, intense in the spectrum of $SS_2D_1$ ($Y_{0.99}Dy_{0.01}(P_{0.8}V_{0.2})O_4$ composition) and rather weak in the other cases, influences the color of the emitted radiation, as evidenced in the chromaticity diagram shown in Fig. 3(b). When this latter emission is weak in fact, the luminescence of the material is yellowish and its representative point moves towards the pure yellow color as the vanadium content of the host, and consequently the Y/B ratio, increases. When strong, it introduces an additional blue component that completely alters the color characteristics giving rise to a bluish luminescence. The presence of this band with proper intensity is necessary in order to

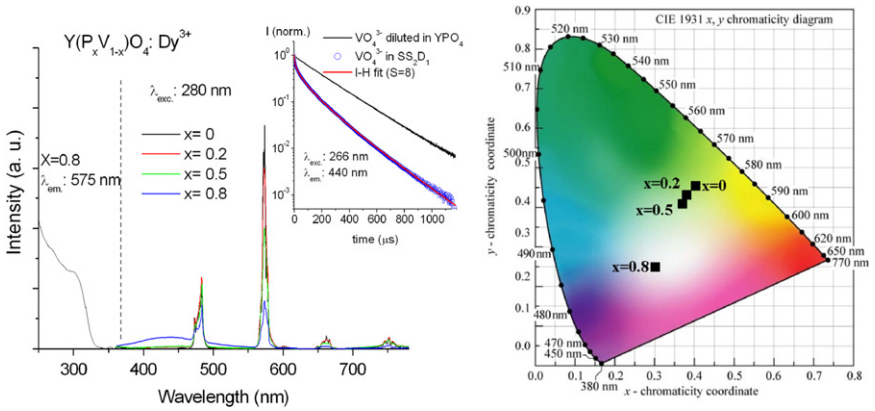


**Fig. 3.** (a) Excitation (representative example) and UV excited emission spectra of the $SS_nD_1$ samples. Inset: $VO_4^{3-}$ decay profiles (see text). (b) Chromaticity coordinates evaluated from the emission spectra.

realize a white emitting phosphor. In summary, the color of the luminescence of this material result from different concomitant processes: the matrix effect on the Y/B intensity ratio, already discussed, the concentration quenching of the vanadate emission and the $VO_4^{3-} \rightarrow Dy^{3+}$ energy transfer. The quenching of the vanadate luminescence is a known phenomenon [21] associated to the migration of the excitation favoring non radiative processes. On the other hand, the mechanism at the origin of the host sensitization of the $Dy^{3+}$ ions has not yet been characterized in details, to the best of our knowledge. In order to investigate this aspect we have measured the decay profile of the vanadate emission of the $SS_2D_1$ sample upon 266 nm pulsed laser excitation (see inset of Fig. 3(a)). We have reproduced the vanadate decay curve using the Inokuti–Hirayama model (Eq. (2)) and considering a D-Q process. The $\tau$ value obtained from the fit is 259 μs (see inset of Fig. 3(a)). The critical distance for the transfer, calculated by means of Eq. (3), is 12 Å. In order to test the applicability of the Hinokuti–Hirayama model in the present case we have measured the decay profile of $VO_4^{3-}$ very diluted (less than 0.5%) into a $YPO_4$ single crystal grown from $Pb_2P_2O_7$ flux. The curve, shown in the inset of Fig. 3(a), is a single exponential with a decay constant of 222 μs, in good agreement with the radiative lifetime provided by the analysis, especially in consideration of the theoretical approximations and of the unavoidable experimental uncertainties. As a last consideration, we point out that the solid state route allows a good control of the stoichiometry and then it is suitable to analyze the relations between structure, composition and spectroscopic properties. On the other hand, it requires high temperature processing that results in a partial sintering of the phosphor grains, whose size and morphology are difficult to control [22]. For this reason we have extended the investigation to other synthetic methodologies.

### 3.2. Sol–gel synthesis and emission performance

The Pechini synthesis route described in Section 2.1 has been adapted from Ref. [4]. The XRD pattern of the resulting powder and its SEM image are reported in Fig. 4. The formation of a single phase system is confirmed as well as the host composition, the broadness of the diffraction peaks indicate that the average size of the grains is smaller than that of the $SS_nD_1$ samples. The SEM image is consistent with this observation and reveals that most of the grains are well crystallizated with the rod-like shape often observed in the case of the macroscopic yttrium phosphate and vanadate crystals grown by spontaneous nucleation from molten salts solutions [23]. The morphology of the particles influences the emission properties: for instance, nano-sized grains allow to realize very homogeneous coatings with high pixel resolution. On the other hand however, the luminescence of a phosphor (in terms of brightness, intensity, etc.) can be affected by phenomena occurring at grain surface like

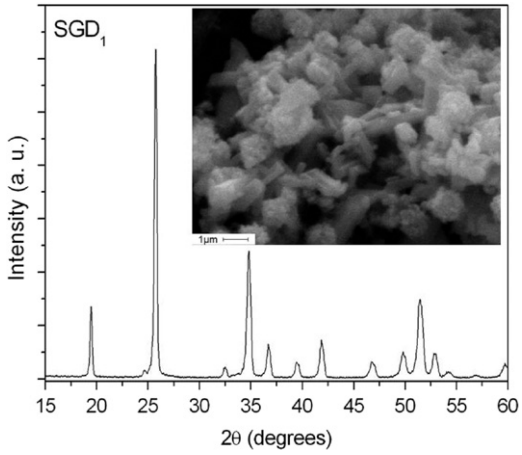


**Fig. 4.** PXRD pattern and SEM image of the $SGD_1$ phosphor.

adsorption of impurities, structural distortions, alterations of the coordination geometries around the active ions, of the electron phonon coupling and of the refractive index [24]. As a consequence, the emission mechanisms in proximity of the grain surface can be different than in the bulk. Concerning the energy transfer processes, the situation is even more complicate: other than the abovementioned effects, boundary effects can modify the excitation profiles of the donor [25] and quantum confinement effects could limit the migration of the energy inside the particles [26]. For these reasons the rationalization of the relationships between the morphology and the luminescence properties is a difficult task and consequently the optimization of the performances requires the application of different experimental techniques depending on the synthetic approach and on the application perspectives of the material. This lies beyond the scope of the present work. Nevertheless, since Bao et al. [4] have pointed out the device potentiality of the phosphor prepared by the sol–gel route, we have decided to compare the emission spectrum of the $SGD_1$ sample with those of a red and a blue commercial phosphors, measured in similar experimental conditions. The result, shown in Fig. 5(a), is encouraging, since the three spectral intensities are of the same order of magnitude. It is interesting to compare the emission properties of $SGD_1$ and $SS_nD_1$ (Fig. 2): the Y/B ratios are similar, the decay time of the $Dy^{3+}$ emission are 348 and 315 μs, respectively, and the total emitted intensity is slightly larger whereas the relative intensity of the vanadate emission is moderately lower in the former case. We suppose that the reason of this behavior could be connected to the different morphologies of the two phosphors: it is conceivable that the better crystallinity and the smaller size of the $SGD_1$ grains can give rise to a brighter luminescence and to a limited

migration of the $Dy^{3+}$ excitation towards killer centers. Consequently, the global intensity of the emitted radiation is higher and its color white, as shown in Fig. 5(b), as an effect of the reduced contribution of the blue component.

### 3.3. Hydrothermal synthesis and comparative evaluation

We have investigated for the first time, to the best of our knowledge, the possibility of applying the hydrothermal method to the synthesis of the $Y_{0.99}Dy_{0.01}(P_{0.8}V_{0.2})O_4$ mixed system. In the frame of the procedure described in Section 2.1, we have monitored the XRD patterns and the emission properties along the various steps of the thermal treatment. The results are shown in Fig. 6. It is evident that the target compound is formed after the low temperature/long time treatment; on the other hand, the broadness of the diffraction peaks indicates a rather small grain size, namely a low crystallinity degree. The intensity of the emission spectrum is low. These properties do not substantially change after the second treatment at 500 °C, whose main purpose is completing the elimination of water and organic residuals. After the annealing at 900 °C the diffraction features become narrower and the luminescence intensity considerably increases. However, compared with the one shown by the previously examined phosphors (see Fig. 7) it remains rather weak, and the color of the emitted radiation is more grayish than white, as already shown in Fig. 5(b). We ascribe this behavior to the low quality of the particle morphology: the SEM image of the $HTD_1$ sample (inset of Fig. 7) in fact reveals the formation of agglomerates of shapeless grains having different sizes. At the present stage, the investigated hydrothemal route has provided an inferior quality phosphor with respect to the solid state and the sol–gel synthesis procedures. Further experiments will be necessary in order to verify the actual reliability of this technique and its perspectives of improvement.

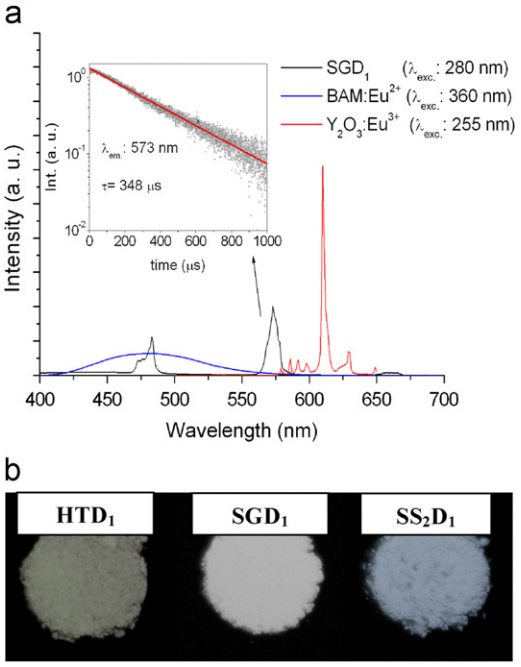


**Fig. 5.** (a) Comparison between the emission spectra of $SGD_1$ and those of the BAM:$Eu^{2+}$ and $Y_2O_3$:$Eu^{3+}$ commercial phosphors. Inset: decay profile of the $Dy^{3+}$ emission in $SGD_1$. (b) Emissions of the $Y_{0.99}Dy_{0.01}(P_{0.8}V_{0.2})O_4$ phosphors upon 254 nm lamp excitation.

## 4. Concluding remarks

In the frame of a comparative study concerning three different methods for the synthesis of the $Y_{0.99}Dy_{0.01}(P_{0.8}V_{0.2})O_4$ phosphor we have explored the relations between host composition, structural and morphological characteristics and emission dynamics.

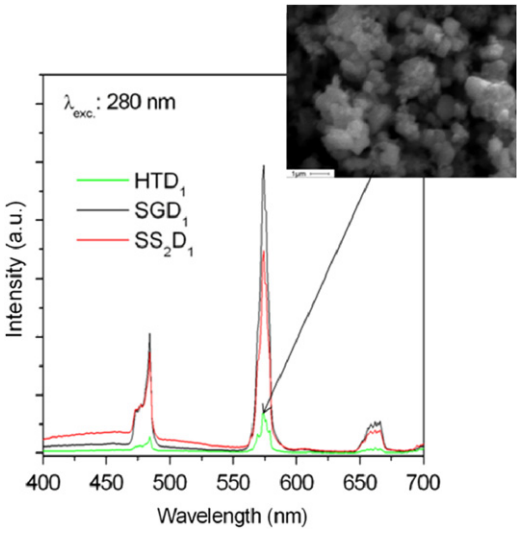


**Fig. 7.** Comparison between the emission spectra of the $Y_{0.99}Dy_{0.01}(P_{0.8}V_{0.2})O_4$ phosphors obtained by the different synthesis methodologies. Inset: SEM image of the $HTD_1$ phosphor.

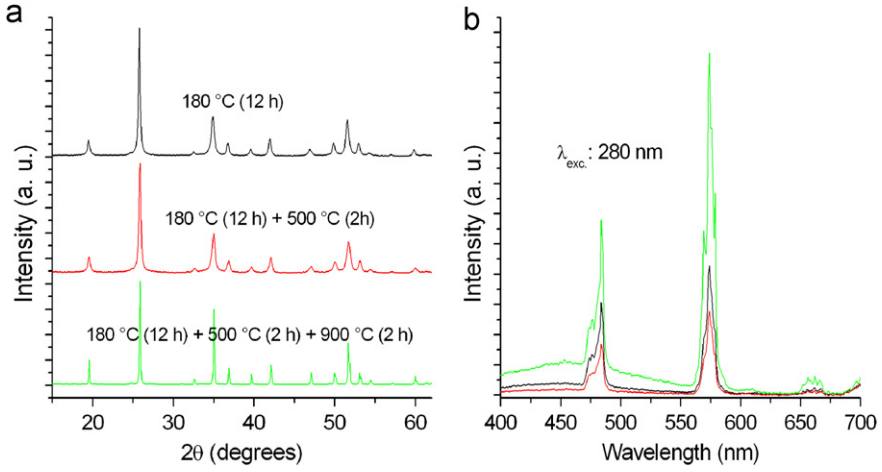


**Fig. 6.** PXRD patterns (a) and emission spectra (b) of the $HTD_1$ phosphor after the different steps of the thermal treatment.

The luminescence properties of this system are the result of the combination of different interacting factors, whose full control is not an easy task. We have demonstrated that not only the intensity ratio between the yellow and blue emission bands of $Dy^{3+}$ depend on the host composition, but also the lifetime of the fluorescent level as well as the efficiency of the energy transfer between the rare earth ions. These effects can be formalized in the framework of the Judd–Ofelt approach, starting from the consideration that the values of the $\Omega_2$ and $\Omega_4$ intensity parameters of the pure phosphate and vanadate lattices are very different. These are related to short range (covalent) effects and long range bulk properties of the local field, and their variation induced by the progressive substitution of phosphor by vanadium (or vice versa) implies the concomitant variation of the polarizability of the oxygen anions and of the local distortion around the optical centers, and then of the oscillator strengths of the radiative transitions. Considering the involved approximations, it is not surprising that the agreement between theory and experiments is more qualitative than quantitative, even if there are reasons to believe that there is room for the improvement of the model. The white luminescence obtained upon UV excitation is the result of the balanced contributions of the host and $Dy^{3+}$ emissions. We have considered the factors affecting the relative intensities, pointing out the key role of the $VO_4^{3-} \rightarrow Dy^{3+}$ energy transfer process, whose mechanism has been characterized. Finally, the tests concerning the three different synthesis methodologies allow to conclude that the adopted solid state, sol–gel and hydrothermal procedures yield the desired phase and composition with good purity. On the other hand, the morphologies of the resulting materials are rather different, and their impact on the luminescence performances is significant: the emissions of the phosphors obtained 'via' sol–gel and solid state reaction have similar intensities but slightly different colors, whereas the phosphor obtained by the hydrothermal route emits rather weakly. The possible reasons of these behaviors have been proposed and briefly discussed.

## References


[1] Z. Hou, P. Yang, C. Li, L. Wang, H. Lian, Z. Quan, J. Lin, Chem. Mater. 20 (2008) 6686.
[2] C.-K. Chang, T.M. Chen, Appl. Phys. Lett. 91 (2007) 081902.
[3] N. Guo, H. You, Y. Song, M. Yang, K. Lin, Y. Zheng, Y. Huang, H. Zheng, J. Mater. Chem. 20 (2010) 9061.
[4] A. Bao, H. Yang, C. Tao, Y. Zhang, L. Han, J. Lumin. 128 (2008) 60.
[5] B. Yan, X.-Q. Su, J. Alloys Compd. 431 (2007) 342.
[6] A.C. Larson, R.B. Von Dreele, General Structure Analysis System (GSAS), Los Alamos National Laboratory Report LAUR 86-748, 2000.
[7] H.B. Toby, J. Appl. Cryst. 34 (2001) 210.
[8] W.O. Milligan, D.F. Mullica, G.W. Beall, L.A. Boatner, Inorg. Chim. Acta 60 (1982) 39.
[9] B.C. Chakoumakos, M.M. Abraham, L.A. Boatner, J. Solid State Chem. 109 (1994) 197.
[10] R.D. Shannon, C.T. Prewitt, Acta Cryst. B 25 (1969) 925.
[11] B.R. Judd, Phys. Rev. 127 (1962) 750.
[12] G.S. Ofelt, J. Chem. Phys. 37 (1962) 511.
[13] E. Cavalli, M. Bettinelli, A. Belletti, A. Speghini, J. Alloys Compd. 341 (2002) 107.
[14] R. Faoro, F. Moglia, M. Tonelli, N. Magnani, E. Cavalli, J. Phys. Condens. Matter 21 (2009) 275501.
[15] A.A. Kaminskii, Crystalline Lasers: Physical Processes and Operating Schemes, CRC Press, New York, 1996.
[16] G. Pan, H. Song, Q. Dai, R. Qin, X. Bai, B. Dong, L. Fan, F. Wang, J. Appl. Phys. 104 (2008) 084910.
[17] S. Shionoya, W.M. Yen, Phosphor Handbook, CRC Press, Boca Raton, FL, 1999.
[18] S. Bigotta, M. Tonelli, E. Cavalli, A. Belletti, J. Lumin. 130 (2010) 13.
[19] E. Cavalli, E. Bovero, A. Belletti, J. Phys. Condens. Matter 14 (2002) 5221.
[20] M. Inokuti, F. Hirayama, J. Chem. Phys. 43 (1965) 1978.
[21] H. Ronde, G. Blasse, J. Inorg. Nucl. Chem. 40 (1978) 215.
[22] S. Ye, F. Xiao, Y.X. Pan, Y.Y. Ma, Q.Y. Zhang, Mater. Sci. Eng. R 71 (2010) 1.
[23] G. Garton, S.H. Smith, B.M. Wanklyn, J. Cryst. Growth 13/14 (1972) 588.
[24] B.M. Tissue, J. Lumin. 131 (2011) 362.
[25] W. Xu, Y. Wang, X. Bai, B. Dong, Q. Liu, J. Chen, H. Song, J. Phys. Chem. C 114 (2010) 14018.
[26] A. Huignard, V. Buissette, A.-C. Franville, T. Gacoin, J.-P. Boilot, J. Phys. Chem. B 107 (2003) 6754.